ACS APPLIED MATERIALS & INTERFACES

Research Article

www.acsami.org

In Situ Synthesis of NiS Nanowall Networks on Ni Foam as a TCO-Free Counter Electrode for Dye-Sensitized Solar Cells

Weijun Ke,[†,‡] Guojia Fang,*[,†,‡] Hong Tao,[†] Pingli Qin,[†] Jing Wang,[†] Hongwei Lei,[†] Qin Liu,[†] and Xingzhong Zhao[†]

[†]Key Laboratory of Artificial Micro- and Nano-structures of Ministry of Education of China, Department of Electronic Science and Technology, School of Physics and Technology, Wuhan University, Wuhan 430072, People's Republic of China

[‡]Wuhan University, Shenzhen Institute, Shenzhen 518055, People's Republic of China

ABSTRACT: Nickel sulfide (NiS) nanowall networks have been prepared by a novel one-step hydrothermal method on a nickel (Ni) foam substrate. The Ni foam has a high conductivity and porous structure. To our knowledge, the Ni foam is used as a conductive substrate for the dye-sensitized solar cell (DSSC) for the first time. The Ni foam is used as not only the conductive substrate but also the Ni sources of the reaction. The Ni foam supported NiS prepared by this simple hydrothermal method shows high catalytic activity for reduction of triiodide ions. The DSSC with a transparent conductive oxide (TCO)-free NiS counter electrode (CE) was herein developed and showed a higher power conversion efficiency of 8.55% than that with a TCO supported NiS CE (7.47%) and a TCO supported platinum CE (7.99%).

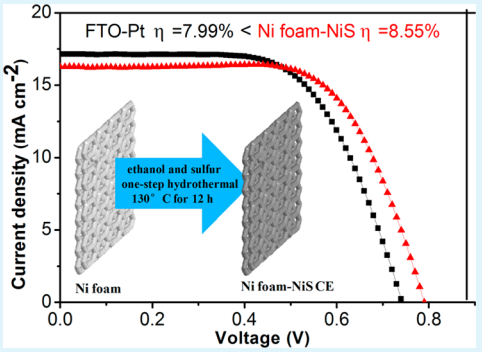

KEYWORDS: *dye-sensitized solar cells, nickel sulfide, nickel foam, counter electrode*

1. INTRODUCTION

Dye-sensitized solar cells (DSSCs) have attracted extensive attention in recent years due to their high conversion efficiency, easy fabrication, and low cost.[1−3] The conventional DSSC has a sandwich-type structure consisting of a counter electrode (CE), an electrolyte, and a dye-sensitized photoanode. As a crucial component, the CE collects electrons from the external circuit and promotes the regeneration of I^- from I_3^-.[4,5] An efficient CE should have good stability, high electrical conductivity, and excellent electrocatalytic activity.[6] The standard CE used in DSSCs is transparent conductive oxide (TCO) supported platinum (Pt), which is normally prepared by a sputting or thermally drying method. A TCO supported Pt CE has high conductivity, excellent electrocatalytic activity, and good chemical stability.[7] However, the limited availability and high price of TCO and noble Pt restrict the large-scale application of DSSCs.[8−11] TCO-free electrodes are meaningful to produce low-cost flexible DSSCs.[12,13] Therefore, an inexpensive and high-performance substitute for TCO supported Pt CEs is highly desirable. On one hand, the TCO substrate has been replaced with a conducting plastic film, a nickel (Ni) sheet, and a stainless steel substrate.[14,15] The power conversion efficiency (PCE) of the DSCS based on the CE with the metal substrate was comparable to that with the fluorine-doped tin oxide (FTO) glass substrate. The Ni sheet substrate supported Pt CE has been demonstrated to be stable in the electrolyte.[7,14,15] On the other hand, the noble Pt was replaced by many low-cost materials, such as conducting polymers,[16] graphene,[17−19] nitrides,[20,21] sulfides,[6,22,23] and carbon.[19,24,25] A hydrothermal approach for in situ growth of metal selenides ($Co_{0.85}Se$ and $Ni_{0.85}Se$) on conductive glass substrates had been used by Wang's group.[26] The DSSC based on $Co_{0.85}Se$ CE achieved a PCE of 9.4%. The hydrothermal approach is mild, facile, and low cost. Nickel sulfide (NiS) possesses good electrocatalytic activity.[27−30] The NiS CEs prepared by a traditional electrodeposition method have been reported.[31,32] The DSSC based on a NiS CE electrodeposited by a potential reversal technique showed a comparable performance (6.82%) to the cell assembled with a Pt CE (7.00%).[31] Highly transparent NiS CEs were prepared by an electrodeposition technique and presented a good photovoltaic performance for thiolate/disulfide mediated DSSCs.[32] Therefore, NiS is a good candidate for an efficient CE. The TCO supported NiS CE was traditionally prepared by an electrodeposition method. However, there is still no report on in situ synthesis of NiS on Ni foam as a CE for DSSCs so far.

In this paper, we report a new method to prepare a novel structure of NiS on Ni foam as a CE. A novel one-step hydrothermal reaction of Ni foam with sulfur was used to prepare NiS nanowall networks. The Ni foam was used as not only the conductive substrate but also the Ni sources of the reaction. The Ni foam, sulfur powders, and ethanol are low-cost and environmentally friendly. Furthermore, a maximum PCE of 8.55% has been received for the DSSC based on the TCO-free and Pt-free NiS CEs, which is higher than that of cells

Received: December 21, 2013
Accepted: March 24, 2014
Published: March 24, 2014

   dx.doi.org/10.1021/am4059155 | ACS Appl. Mater. Interfaces 2014, 6, 5525−5530

assembled with a TCO supported NiS CE (7.47%) or a platinum CE (7.99%).

2. EXPERIMENTAL DETAILS

2.1. Materials. Sulfur powders, hydrogen hexachloroplatinate(IV), ethanol, nitric acid, diethanol amine, tetrabutyl titanate, thioacetamide, polyethylene glycol, and glacial acetic acid were purchased from Sinopharm Chemical Reagent Co., Ltd. Guanidine thiocyanate (GuSCN), 4-*tert*-butylpyridine (TBP), iodine (I_2) and 1-methyl-3-propyl imidazolium iodide (PMII) were purchased from Aladdin Industrial Corporation. Titanium isopropoxide and lithium iodide (LiI, 99.99%) were purchased from Acros. FTO (sheet resistance 14 Ω sq^{-1}) and N719 were purchased from Asahi Glass (Japan) and Solaronix (Switzerland), respectively. The Ni foam was purchased from Beijing Yuceda Trade Co., Ltd. The pore size, porosity, thickness, and purity of Ni foam are 0.2 mm, 95%, 0.5 mm, and 99.5%, respectively. All the used reagents were analytical grade, without further purification.

2.2. Fabrication of TiO_2 Photoanodes. The photoanodes were prepared according to a standard procedure that has been reported in our previous work.[33] Firstly, a 50 nm thick compact TiO_2 film was coated on FTO by using a spin-coating method and then heated to 550 °C for 30 min in air. Secondly, a 12 μm thick porous TiO_2 film was coated on compact TiO_2 film by using a doctor-blade method and then sintered at 500 °C for 30 min in air. Finally, a 6 μm thick scattering layer was coated on porous TiO_2 film by using a doctor-blade method and then sintered at 500 °C for 30 min in air too. To absorb the dye adequately, the film was kept at 60 °C for 12 h in a 0.3 mM N719 anhydrous ethanol solution.

2.3. Fabrication of CEs. A FTO supported NiS (FTO-NiS) CE was prepared by the following processes, which is similar to our previous work.[33] Firstly, a 1 μm thick Ni film was coated on FTO by radio frequency (RF) magnetron sputtering from a Ni target (99.99% purity) at room temperature. The film was deposited at a RF power of 100 W and sputtering pressure of 1 Pa. Secondly, 0.03 g of sulfur powders, the prepared Ni film, and 50 mL of ethanol were put into a 100 mL Teflon-lined autoclave. To form NiS, the Ni film was kept in the autoclave at 130 °C for 12 h. The film was washed by ethanol several times and finally heated to 50 °C for 1 h in air. An FTO supported Pt (FTO-Pt) CE was prepared by RF magnetron sputtering from a Pt target (99.99% purity) in the optimum conditions. A Ni foam supported NiS (Ni-NiS) CE was prepared by putting 0.03 g of sulfur powders, 50 mL of ethanol, and the clean Ni foam into a 100 mL Teflon-lined autoclave directly. The reaction was kept at 130 °C for 12 h. The film was washed with ethanol several times and finally heated to 50 °C for 1 h in air.

2.4. Characteristics. The morphology of FTO-NiS and Ni-NiS CEs was observed by a high-resolution field emission scanning electron microscope (FEI Nova Nano-SEM 450). Transmission electron microscopy (TEM) images were taken on a JEOL-2010 TEM operated at 200 kV. The chemical states and compositions of the CuS films were characterized by X-ray photoelectron spectroscopy (XPS, Thermo Scientific, Escalab 250Xi). Film crystal structure was examined by X-ray diffraction (XRD, Bruker Axs, D8 Advance) with Cu Kα radiation under operation conditions of 40 kV and 40 mA. The DSSC was assembled with a photoanode, an electrolyte, and a CE. A Surlyn film was used to separate the CE and the photoanode. The back of the porous Ni-NiS CE was covered with a piece of glass sheet, so the leakage of the liquid electrolyte through the porous Ni-NiS CE without FTO did not occur. The electrolyte contains 0.5 M TBP, 0.1 M GuSCN, 0.03 M I_2, 0.04 M LiI, and 1 M PMII in propylene carbonate and acetonitrile (1:1 in volume ratio). A 0.25 cm^2 mask was used to control the irradiated area. A standard ABET Sun 2000 Solar Simulator with a power density of 100 mW cm^{-2} (AM1.5 simulated irradiation) was used to irradiate the prepared DSSCs. The scan rate was 10 mV s^{-1}. A symmetrical dummy cell (CE/electrolyte/CE) in the dark was used to perform the Tafel polarization measurements, EIS experiments, and CV. The effective area of the symmetrical cell was 0.25 cm^2. A CHI660D electrochemical workstation (ShangHai, China) was used to measure the cyclic voltammetry (CV), electrochemical impedance spectroscopy (EIS), Tafel polarization measurement, and photocurrent density–voltage (J–V) characteristics. The EIS measurement was performed with a frequency ranging from 100 kHz to 0.1 Hz at zero bias, and the AC amplitude was set at 10 mV. The Tafel polarization measurements and CV were carried out with a scan rate of 10 mV s^{-1}.

3. RESULTS AND DISCUSSION

The sandwich-type structure of the DSSC based on a Ni-NiS CE is shown in Figure 1. The SEM and TEM images of FTO-

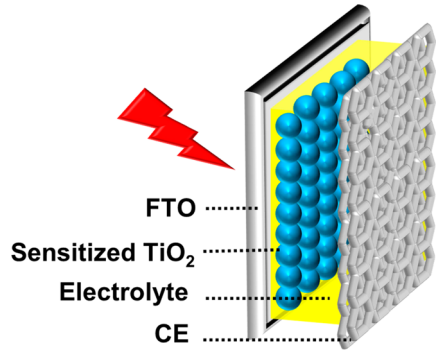

Figure 1. Schematic illustration of the structure of the DSSC.

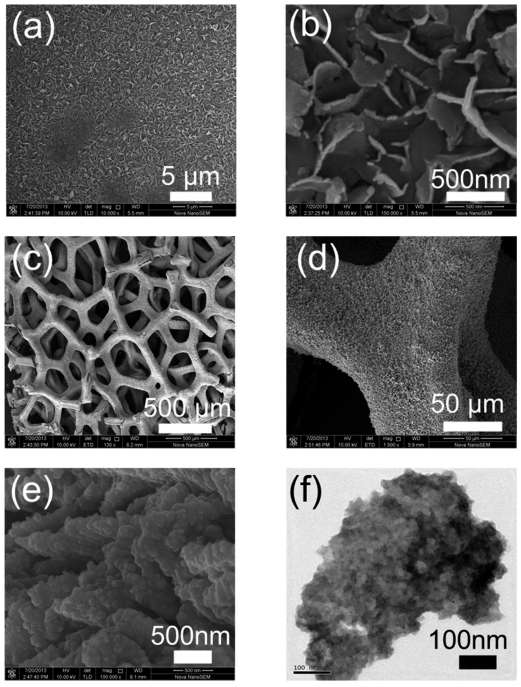

Figure 2. SEM images of FTO-NiS (a, b) and Ni-NiS (c–e) CEs at different magnifications. TEM image of Ni-NiS (f).

NiS and Ni-NiS CEs are shown in Figure 2. Figure 2a,b shows the images of the FTO-NiS CE at a low magnification and high magnification, respectively. The NiS electrode film is uniformly distributed on FTO, which featured a nanowall network-like shape. Figure 2c–e shows the images of Ni-NiS CEs at different magnifications. As shown in Figure 2c, the Ni foam has a porous network structure. The surface of the Ni foam has been fully covered with NiS (Figure 2d). The NiS has a regular

dx.doi.org/10.1021/am4059155 | ACS Appl. Mater. Interfaces 2014, 6, 5525–5530

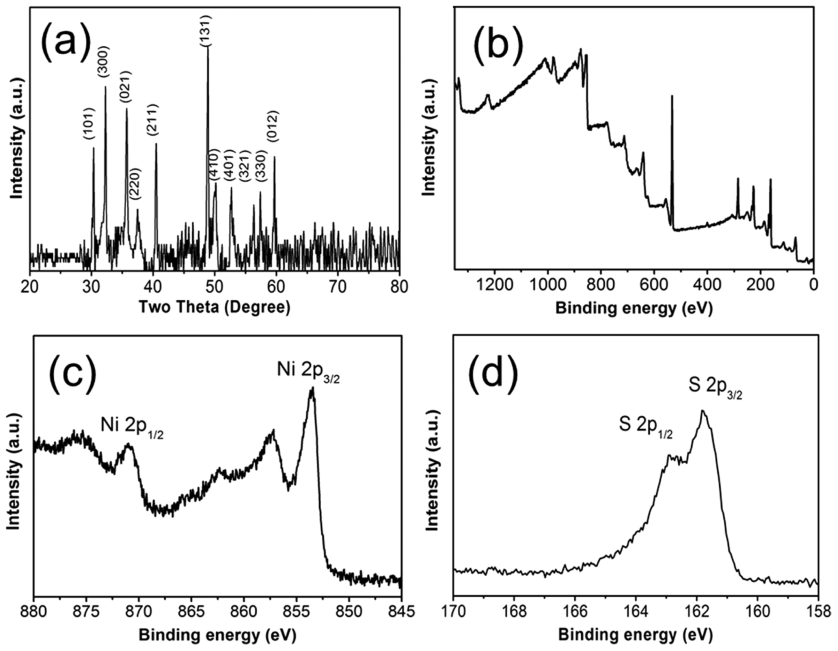

Figure 3. (a) XRD pattern of NiS nanowall networks. (b) XPS survey spectrum of NiS nanowall networks. XPS spectra of (c) Ni and (d) S of NiS nanowall networks.

nanowall network structure (Figure 2e). As shown in Figure 2f, the NiS nanowall has many nanoparticles on its surface. We attribute the formation of the NiS nanowall to a typical Ostwald ripening process, according to our previous work.[33] The sulfur powders reacted with Ni on the surface of the Ni foam. A nucleus was formed and then followed by crystal growth. The Ni foam has enough Ni source. A secondary growth process may have occurred, which results in nucleation/growth on the sidewall surface of the NiS nanowall. Therefore, the NiS nanowall on the Ni foam substrate has many nanoparticles on its surface, which is thicker than that on the FTO substrate. To check the composition and phase structure of NiS nanowall networks, XPS and XRD measurements were carried out. A thick Ni film was coated on a glass sheet substrate by RF magnetron sputtering from a Ni target. The NiS nanowall networks on glass were prepared by a hydrothermal method in the same condition. The NiS powders were peeled off from the as-obtained NiS nanowall networks on glass. The powders were used to measure the phase structure. As shown in Figure 3a, the diffraction peaks of the powdered NiS contain (101), (300), (021), (220), (211), (131), (410), (401), (321), (330), and (012) faces, which confirms the formation of a rhombohedral structured NiS. As shown in Figure 3b, the XPS survey spectrum of as-obtained NiS nanowall networks confirms the presences of Ni and S signals. The binding energies of the S $2p_{1/2}$ and S $2p_{3/2}$ peaks are 162.93 and 161.83 eV, respectively (Figure 3d). The binding energies of the Ni $2p_{1/2}$ and Ni $2p_{3/2}$ peaks are 870.98 and 853.68 eV, respectively (Figure 3c). The result is close to the previous reported values for NiS.[34−36] Therefore, a rhombohedral NiS phase was obtained via this simple hydrothermal process. Figure 4 shows the *J*−*V* curves of DSSCs with FTO-Pt, FTO-NiS, and Ni-NiS CEs. The PCEs of 7.99% and 7.47% are obtained for the DSSCs based on FTO-Pt and FTO-NiS CEs, respectively. The photovoltaic parameters are listed in Table 1. The optimum thickness of Ni film is 1 μm. The sample prepared by a too thick Ni film will have a poor adhesion with the substrate. By the way, the NiS film will be

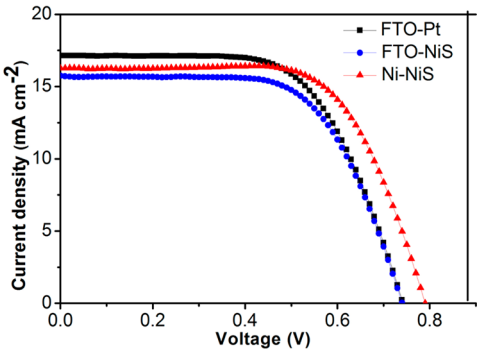

Figure 4. *J*−*V* curves of DSSCs based on FTO-Pt, FTO-NiS, and Ni-NiS CEs.

easy to fall off due to the stress difference between NiS and FTO at a high temperature. If the Ni film is too thin, the catalytic activity of the CE will be poor. When the reaction procedure is finished, the metallic film turned black. It also means that the 1 μm thick Ni film was exhausted after the reaction was kept at 130 °C for 12 h, and the Ni film was converted to NiS completely. The reaction of Ni foam with sulfur lasting 12 h at 130 °C is adequate too. The Ni foam is covered with NiS nanowall networks fully. The reaction becomes very slow after a longer time. Furthermore, the film will be easy to fall off the substrate and the reaction will be too violent at a higher temperature. The Ni film or Ni foam does not react with sulfur at a too low temperature. Therefore, the autoclave duration and temperature presented here is the optimum condition. It is amazing that the DSSC with Ni-NiS CE received a maximum PCE of 8.55%. As shown in Table 1, the DSSC with Ni-NiS CE has a high fill factor and open-circuit voltage. The Ni foam has a better electrical conductivity than that of the FTO. The FTO has a large sheet resistance value (14 Ω sq^{-1}). The CE based on a metal substrate can be aimed at lower-cost markets and applicable for flexible DSSCs.[14,15] It has the merit of improving the PCE, open-circuit voltage, and

dx.doi.org/10.1021/am4059155 | ACS Appl. Mater. Interfaces 2014, 6, 5525−5530

Table 1. Electrochemical and Photovoltaic Parameters of DSSCs Based on FTO-Pt, FTO-NiS, and Ni-NiS CEs

CEs	V_{oc} (V)	J_{sc} (mA cm^{-2})	FF	PCE (%)	R_s (Ω cm^2)	R_{ct} (Ω cm^2)	Z_N (Ω cm^2)
FTO-Pt	0.75	17.13	0.62	7.99	12.55	5.15	9.16
FTO-NiS	0.75	15.75	0.63	7.47	12.56	1.48	8.53
Ni-NiS	0.80	16.26	0.66	8.55	4.95	1.00	5.79

fill factor of the DSSCs by reducing its internal resistance.[14,15] The roles of the CE are to collect electrons from the external circuit and to catalyze the reduction of the redox couple.[4] A porous structure of Ni foam may be beneficial to diffuse the electrolyte, and the three-dimensional structure has a higher surface area than a planar FTO substrate. Therefore, the reduction of triiodide ions is faster. The substrate and NiS have a tight attachment by in situ synthesis of NiS on Ni Foam. The NiS nanowall networks have a high specific area and good catalytic activity. All of these reasons may lead the DSSC based on Ni-NiS CE to have a high fill factor, open-circuit voltage, and PCE. It is obvious that the short-circuit current density of FTO-NiS and Ni-NiS CEs are lower than that of the FTO-Pt CE. We attribute the higher short-circuit current density of the FTO-Pt CE to that light was absorbed again as the thick Pt film on FTO is like a mirror.

To further understand the high electrocatalytic activity of Ni-NiS CE, Tafel polarization measurements, CV, and EIS were measured by using a symmetrical dummy cell.[37] Figure 5 shows

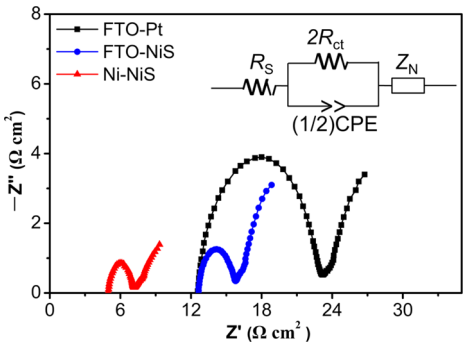

Figure 5. EIS of symmetrical cells fabricated with two identical FTO-Pt, FTO-NiS, and Ni-NiS CEs.

the EIS curves. The inset of Figure 5 shows the equivalent circuit used to fit the experimental EIS data. The ZView software was used to fit the parameters of the Nyquist plots. The charge-transfer resistance (R_{ct}) at the electrolyte/CE interface and the corresponding phase angle element (CPE) give rise to the left semicircle (high frequency region). The high-frequency intercept on the real axis represents the series resistance (R_S). The right incomplete semicircle in the low-frequency range is assigned to impedance related to the finite layer Nernst diffusion impedance (Z_N) within the electrolyte and charge-transfer processes occurring at the electrolyte/CE interface.[20,33,38] The R_S value of Ni-NiS is 4.95 Ω cm^2, which is lower than that of FTO supported CEs. We attribute the low R_S value of Ni-NiS CE to that the Ni foam has a better electrical conductivity than the FTO. The R_{ct} values of Ni-NiS and FTO-NiS are 1.00 and 1.48 Ω cm^2, respectively. However, FTO-Pt CE has a high R_{ct} value (5.15 Ω cm^2). All the values are summarized in Table 1. The catalytic activity of the electrodes can be reflected from the R_{ct} in the electrode/electrolyte interface. This result means that the catalytic activity of the FTO-Pt CE is worse than that of the Ni-NiS CE.

Tafel polarization measurement is an efficient way to reconfirm the electrochemical catalytic activities of CEs.[33] The limiting current density (J_{lim}) and the exchange current density (J_0) are related to the catalytic activity of the catalysts. A large J_{lim} indicates a large diffusion coefficient and a small Z_N. A large J_0 generally means high ability for I_3^- reduction. The J_0 varies inversely with R_{ct}.[33] The values of J_0 and J_{lim} are also in good agreement with the result of EIS measurement, which are according to the following equation[20,33,38]

$$J_0 = RT/nFR_{ct} \quad (1)$$

where F is Faraday's constant, n is the electron number involved in the reaction, T is the absolute temperature, and R is the gas constant. The J_0 can be obtained by eq 1

$$J_{lim} = 2nFCD/l \quad (2)$$

where F is Faraday's constant, n is the electron number involved in the reaction, C is the triiodide concentration, l is the spacer thickness, and D is the diffusion coefficient of the triiodide. The J_{lim} can be obtained by eq 2.

Tafel polarization characterization was carried out in a symmetrical dummy cell similar to the one used in the EIS measurement. As shown in Figure 6a, the cathodic and anodic branches of the Ni-NiS and FTO-NiS CEs exhibit a larger slope than that of the FTO-Pt CE. It indicates that Ni-NiS and FTO-NiS have a high J_{lim} and J_0. Moreover, the J_0 and the J_{lim} of the

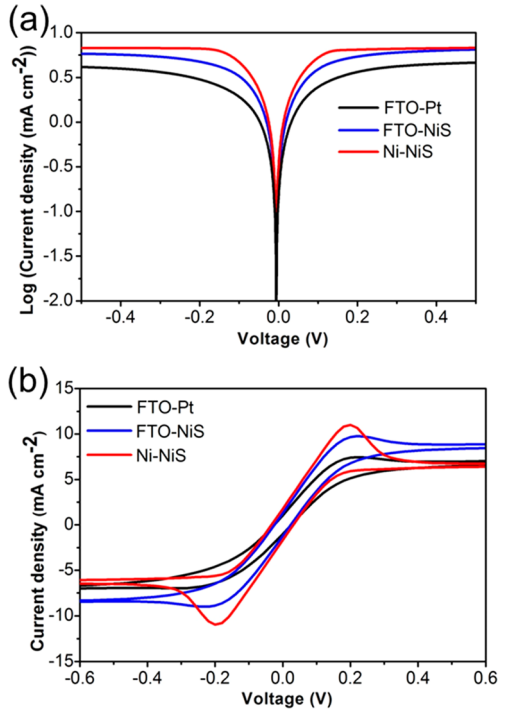

Figure 6. (a) Tafel polarization curves and (b) cyclic voltammetry of symmetrical cells fabricated with two identical FTO-Pt, FTO-NiS, and Ni-NiS CEs.

dx.doi.org/10.1021/am4059155 | ACS Appl. Mater. Interfaces 2014, 6, 5525−5530

Ni-NiS are the highest. A larger J_0 means that Ni-NiS CE has a better catalytic activity for I_3^- reduction.

The electrochemical catalytic activities of NiS and Pt CEs, which is crucial for CEs used in DSCs, are examined by cyclic voltammetry under an I^-/I_3^- electrochemical system with the symmetrical dummy cells which is the same one used in the Tafel polarization and EIS measurements (Figure 6b). It is well-known that triiodide is reduced to iodide on the CE surface ($I_3^- + 2e^- \rightarrow 3I^-$).[39] The inverse slope of a voltammogram at the potential of 0 V characterizes the catalytic activity of an electrode.[40−43] The FTO-NiS and Ni-NiS CEs show a good catalytic activity for the I_3^- reduction with a sharp slope. Furthermore, the Ni-NiS CE has a higher current density than the FTO-NiS and FTO-Pt CEs, indicating that a faster rate for triiodide reduction reaction can be presented, which is in accordance with the EIS and Tafel polarization measurement results. It means that Pt film has a worse catalytic activity than NiS nanowall network film on Ni foam. Therefore, the PCE of the FTO-Pt CE is lower than that of the Ni-NiS CE. In consideration of the high PCE and simple method, the NiS nanowall network film on Ni foam is a good candidate as a TCO-free and Pt-free CE.

4. CONCLUSION

In conclusion, NiS nanowall networks on FTO and Ni foam were prepared by a novel and facile one-step hydrothermal reaction of Ni foam with sulfur. The electrochemical results reveal that the Ni-NiS CE has a good catalytic activity for the I_3^- reduction. The Ni-NiS CE has a good electrocatalytic activity. The DSSC with Ni-NiS CE received a higher PCE of 8.55% than that with FTO-Pt CE (7.99%), suggesting that Ni-NiS CE is an extremely interesting alternative to FTO-Pt CE for DSSCs. Furthermore, the Ni foam is bendable. A flexible and stable substrate is much desired for mass production of DSSCs. Therefore, it is of significance to fabricate a low-cost, large-area, and flexible DSSC with the TCO- and Pt-free CE.

AUTHOR INFORMATION

Corresponding Author

*Tel: +86 (0)27 68752147. Fax: +86 (0)27 68752569. E-mail: gjfang@whu.edu.cn.

Notes

The authors declare no competing financial interest.

ACKNOWLEDGMENTS

This work was supported by the National Basic Research Program (No. 2011CB933300) of China, Shenzhen Strategic Emerging Industry Development Funds (JCYJ20130401160028796), and the Research Program of Wuhan Science & Technology Bureau (2013010501010141).

REFERENCES

(1) O'Regan, B.; Grätzel, M. A low-cost, high-efficiency solar cell based on dye-sensitized colloidal TiO_2 films. *Nature* **1991**, *353*, 24.

(2) Grätzel, M. Photoelectrochemical cells. *Nature* **2001**, *414*, 338−344.

(3) Yella, A.; Lee, H. W.; Tsao, H. N.; Yi, C.; Chandiran, A. K.; Nazeeruddin, M. K.; Diau, E. W.; Yeh, C. Y.; Zakeeruddin, S. M.; Gratzel, M. Porphyrin-sensitized solar cells with cobalt (II/III)-based redox electrolyte exceed 12 percent efficiency. *Science* **2011**, *334*, 629−634.

(4) Grätzel, M. Dye-sensitized solar cells. *J. Photochem. Photobiol., C* **2003**, *4*, 145−153.

(5) Hagfeldt, A.; Boschloo, G.; Sun, L.; Kloo, L.; Pettersson, H. Dye-sensitized solar cells. *Chem. Rev.* **2010**, *110*, 6595−6663.

(6) Yao, R. Y.; Zhou, Z. J.; Hou, Z. L.; Wang, X.; Zhou, W. H.; Wu, S. X. Surfactant-free $CuInS_2$ nanocrystals: An alternative counter-electrode material for dye-sensitized solar cells. *ACS Appl. Mater. Interfaces* **2013**, *5*, 3143−3148.

(7) Murakami, T. N.; Grätzel, M. Counter electrodes for DSC: Application of functional materials as catalysts. *Inorg. Chim. Acta* **2008**, *361*, 572−580.

(8) Papageorgiou, N. Counter-electrode function in nanocrystalline photoelectrochemical cell configurations. *Coord. Chem. Rev.* **2004**, *248*, 1421−1446.

(9) Greijer, H.; Karlson, L.; Lindquist, S. E.; Hagfeldt, A. Environmental aspects of electricity generation from a nanocrystalline dye sensitized solar cell system. *Renewable Energy* **2001**, *23*, 27−39.

(10) Smestad, G.; Bignozzi, C.; Argazzi, R. Testing of dye sensitized TiO_2 solar cells I: Experimental photocurrent output and conversion efficiencies. *Sol. Energy Mater. Sol. Cells* **1994**, *32*, 259−272.

(11) Veerappan, G.; Bojan, K.; Rhee, S. W. Sub-micrometer-sized graphite as a conducting and catalytic counter electrode for dye-sensitized solar cells. *ACS Appl. Mater. Interfaces* **2011**, *3*, 857−862.

(12) Cha, S. I.; Kim, Y.; Hwang, K. H.; Shin, Y. J.; Seo, S. H.; Lee, D. Y. Dye-sensitized solar cells on glass paper: TCO-free highly bendable dye-sensitized solar cells inspired by the traditional Korean door structure. *Energy Environ. Sci.* **2012**, *5*, 6071.

(13) Fu, D.; Lay, P.; Bach, U. TCO-free flexible monolithic back-contact dye-sensitized solar cells. *Energy Environ. Sci.* **2013**, *6*, 824.

(14) Fang, X. M.; Ma, T. L.; Akiyama, M.; Guan, G. Q.; Tsunematsu, S.; Abe, E. Flexible counter electrodes based on metal sheet and polymer film for dye-sensitized solar cells. *Thin Solid Films* **2005**, *472*, 242−245.

(15) Ma, T. L.; Fang, X. M.; Akiyama, M.; Inoue, K.; Noma, H.; Abe, E. Properties of several types of novel counter electrodes for dye-sensitized solar cells. *J. Electroanal. Chem.* **2004**, *574*, 77−83.

(16) Tai, Q. D.; Chen, B. L.; Guo, F.; Xu, S.; Hu, H.; Sebo, B.; Zhao, X. Z. In situ prepared transparent polyaniline electrode and its application in bifacial dye-sensitized solar cells. *ACS Nano* **2011**, *5*, 3795−3799.

(17) Tjoa, V.; Chua, J.; Pramana, S. S.; Wei, J.; Mhaisalkar, S. G.; Mathews, N. Facile photochemical synthesis of graphene-Pt nanoparticle composite for counter electrode in dye sensitized solar cell. *ACS Appl. Mater. Interfaces* **2012**, *4*, 3447−3452.

(18) Roy-Mayhew, J. D.; Boschloo, G.; Hagfeldt, A.; Aksay, I. A. Functionalized graphene sheets as a versatile replacement for platinum in dye-sensitized solar cells. *ACS Appl. Mater. Interfaces* **2012**, *4*, 2794−2800.

(19) Miao, X. H; Pan, K.; Pan, Q. J.; Zhou, W.; Wang, L.; Liao, Y. P.; Tian, G. H.; Wang, G. F. Highly crystalline graphene/carbon black composite counter electrodes with controllable content: Synthesis, characterization and application in dye-sensitized solar cells. *Electrochim. Acta* **2013**, *96*, 155−163.

(20) Wu, M. X.; Lin, X.; Wang, Y. D.; Wang, L.; Guo, W.; Qi, D.; Peng, X. J.; Hagfeldt, A.; Gratzel, M.; Ma, T. L. Economical Pt-free catalysts for counter electrodes of dye-sensitized solar cells. *J. Am. Chem. Soc.* **2012**, *134*, 3419−3428.

(21) Jiang, Q. W.; Li, G. R.; Gao, X. P. Highly ordered TiN nanotube arrays as counter electrodes for dye-sensitized solar cells. *Chem. Commun.* **2009**, 6720−6722.

(22) Wu, J. H.; Yue, G. T.; Xiao, Y. M.; Huang, M. L.; Lin, J. M.; Fan, L. Q.; Lan, Z.; Lin, J. Y. Glucose aided preparation of tungsten sulfide/multi-wall carbon nanotube hybrid and use as counter electrode in dye-sensitized solar cells. *ACS Appl. Mater. Interfaces* **2012**, *4*, 6530−6536.

(23) Miao, X. H.; Pan, K.; Wang, G. F.; Liao, Y. P.; Wang, L.; Zhou, W.; Jiang, B. J.; Pan, Q. J.; Tian, G. H. Well-dispersed CoS nanoparticles on a functionalized graphene nanosheet surface: A counter electrode of dye-sensitized solar cells. *Chem.—Eur. J.* **2014**, *20*, 474−482.

(24) Bu, C. H.; Liu, Y. M.; Yu, Z. H.; You, S. J.; Huang, N.; Liang, L. L.; Zhao, X. Z. Highly transparent carbon counter electrode prepared via an in situ carbonization method for bifacial dye-sensitized solar cells. *ACS Appl. Mater. Interfaces* **2013**, *5*, 7432−7438.
(25) Liao, Y. P.; Pan, K.; Wang, L.; Pan, Q. J.; Zhou, W.; Miao, X. H.; Jiang, B. J.; Tian, C. G.; Tian, G. H.; Wang, G. F.; Fu, H. G. Facile synthesis of high-crystallinity graphitic carbon/Fe_3C nanocomposites as counter electrodes for high-efficiency dye-sensitized solar cells. *ACS Appl. Mater. Interfaces* **2013**, *5*, 3663−3670.
(26) Gong, F.; Wang, H.; Xu, X.; Zhou, G.; Wang, Z. S. In situ growth of $Co_{0.85}Se$ and $Ni_{0.85}Se$ on conductive substrates as high-performance counter electrodes for dye-sensitized solar cells. *J. Am. Chem. Soc.* **2012**, *134*, 10953−10958.
(27) Zhao, W.; Zhu, X. L.; Bi, H.; Cui, H. L.; Sun, S. R.; Huang, F. Q. Novel two-step synthesis of NiS nanoplatelet arrays as efficient counter electrodes for dye-sensitized solar cells. *J. Power Sources* **2013**, *242*, 28−32.
(28) Li, Z. Q.; Gong, F.; Zhou, G.; Wang, Z. S. NiS_2/reduced graphene oxide nanocomposites for efficient dye-sensitized solar cells. *J. Phys. Chem. C* **2013**, *117*, 6561−6566.
(29) Zhao, W.; Lin, T. Q.; Sun, S. R.; Bi, H.; Chen, P.; Wan, D. Y.; Huang, F. Q. Oriented single-crystalline nickel sulfide nanorod arrays: "Two-in-one" counter electrodes for dye-sensitized solar cells. *J. Mater. Chem. A* **2013**, *1*, 194.
(30) Zhang, L. L.; Mulmudi, H. K.; Batabyal, S. K.; Lam, Y. M.; Mhaisalkar, S. G. Metal/metal sulfide functionalized single-walled carbon nanotubes: FTO-free counter electrodes for dye sensitized solar cells. *Phys. Chem. Chem. Phys.* **2012**, *14*, 9906−9911.
(31) Sun, H. C.; Qin, D.; Huang, S. Q.; Guo, X. Z.; Li, D. M.; Luo, Y. H.; Meng, Q. B. Dye-sensitized solar cells with NiS counter electrodes electrodeposited by a potential reversal technique. *Energy Environ. Sci.* **2011**, *4*, 2630.
(32) Ku, Z. L.; Li, X.; Liu, G. H.; Wang, H.; Rong, Y. G.; Xu, M.; Liu, L. F.; Hu, M.; Yang, Y.; Han, H. W. Transparent NiS counter electrodes for thiolate/disulfide mediated dye-sensitized solar cells. *J. Mater. Chem. A* **2013**, *1*, 237.
(33) Ke, W. J.; Fang, G. J.; Lei, H. W.; Qin, P. L.; Tao, H.; Zeng, W.; Wang, J.; Zhao, X. Z. An efficient and transparent CuS nanosheet film counter electrode for bifacial quantum dot−sensitized solar cells. *J. Power Sources* **2014**, *248*, 809−815.
(34) Yang, P. F.; Song, B.; Wu, R.; Zheng, Y. F.; Sun, Y. F.; Jian, J. K. Solvothermal growth of NiS single-crystalline nanorods. *J. Alloys Compd.* **2009**, *481*, 450−454.
(35) Chen, N.; Zhang, W. Q.; Yu, W. C.; Qian, Y. T. Synthesis of nanocrystalline NiS with different morphologies. *Mater. Lett.* **2002**, *55*, 230−233.
(36) Yan, S. C.; Shi, Y.; Sun, L. T.; Xiao, Z. D.; Sun, B.; Xu, X. Controlled synthesis of NiS nanoparticle/CdS nanowire heterostructures via solution route and their optical properties. *Mater. Sci. Eng., B* **2013**, *178*, 109−116.
(37) Zeng, W.; Fang, G. j.; Wang, X. Q.; Zheng, Q.; Li, B. R.; Huang, H. H.; Tao, H.; Liu, N. S.; Xie, W. J.; Zhao, X. Z.; Zou, D. C. Hierarchical porous nano-carbon composite: Effective fabrication and application in dye sensitized solar cells. *J. Power Sources* **2013**, *229*, 102−111.
(38) Gong, F.; Xu, X.; Li, Z.; Zhou, G.; Wang, Z. S. $NiSe_2$ as an efficient electrocatalyst for a Pt-free counter electrode of dye-sensitized solar cells. *Chem. Commun.* **2013**, *49*, 1437−1439.
(39) Ferber, J.; Stangl, R.; Luther, J. An electrical model of the dye-sensitized solar cell. *Sol. Energy Mater. Sol. Cells* **1998**, *53*, 29−54.
(40) Liberatore, M.; Petrocco, A.; Caprioli, F.; La Mesa, C.; Decker, F.; Bignozzi, C. A. Mass transport and charge transfer rates for Co(III)/Co(II) redox couple in a thin-layer cell. *Electrochim. Acta* **2010**, *55*, 4025−4029.
(41) Kavan, L.; Yum, J. H.; Grätzel, M. Graphene nanoplatelets outperforming platinum as the electrocatalyst in co-bipyridine-mediated dye-sensitized solar cells. *Nano Lett.* **2011**, *11*, 5501−5506.
(42) Huang, S. Q.; Sun, H. C.; Huang, X. M.; Zhang, Q. X.; Li, D. M.; Luo, Y. H.; Meng, Q. B. Carbon nanotube counter electrode for high-efficient fibrous dye-sensitized solar cells. *Nanoscale Res. Lett.* **2012**, *7*, 1−7.
(43) Kavan, L.; Yum, J. H.; Grätzel, M. Optically transparent cathode for dye-sensitized solar cells based on graphene nanoplatelets. *ACS Nano* **2010**, *5*, 165−172.